Complementary method used for noninvasive evaluation of some medical prostheses

Adriana Savin [1], Mihail Liviu Craus [1,2], Rozina Steigmann[1],
Vitalii Turchenko [2], Alina Bruma [3], Tatiana E. Konstantinova [4]
1 National Institute for Research and Development for Technical Physics, Iasi, Romania
2 Joint Institute for Nuclear Research, Dubna Russia
3 National Institute of Standards and Technology, Gaithersburg, MD USA
4 Donetsk Institute for Physics and Engineering named after O.O. Galkin of National Academy of Sciences of Ukraine, Donetsk, Ukraine

Abstract

The paper proposes the investigation of influence of addition of Ce ions to the phase stability and mechanical properties of Zr - based ceramics for potential applications in the biomedical field. The structural investigation are based on X-ray and neutron diffraction in order to establish a first indication of the variation of the phase composition and structural parameters, as well as nondestructive evaluation, using resonant ultrasound spectroscopy, in order to establish a correlation between the structural parameters and mechanical properties of the sample.

1. Introduction

Medical ceramics include a wide range of bioactive composites such as a glasses, glass-ceramics and ceramic- polymers. Biocompatibility and resistance to mechanical stress are one of the most important features when designing new materials based on ceramics for medical implants. Rheumatoid arthritis characterized by synovial inflammation, damage to both cartilage and bone advertising leads to symptoms which can appear in different forms, as rigidity, deformity, limb shortening or movement reduction. Symptoms such as pain and loss of functions justify ultimately total hip arthroplasty (THA). THA is the solution preferred to improved health – related quality of life [1,2]. However clarification is still required used annual rates of THA[3]. Over last decades, THA has become one the most successful surgical operations and it is known that metals and metal alloys are greatly used in orthopedic implants. Ceramic technology continues to evolve, new materials based on ceramics composites with surface modifications offer more options to the THA surgery[4]. Zirconia (ZrO_2)-based ceramics are preferred due to their advanced mechanical properties such as high-fracture toughness and bulk modulus, corrosion resistance, high dielectric constant, chemical inertness, low chemical conductivity and biocompatibility. It has been show that, at ambient pressure, pure Zirconia exhibits three crystallographic structures, their occurrence depending on the temperature - the monoclinic state, $P2_{1/c}$; the tetragonal phase, $P4_{2/nmc}$ and the cubic, Fm-3m phase [5]. For temperatures up to 1180^0C, the symmetry of the crystal is monoclinic, with the space group, $P2_{1/c}$. Under external stress, as grinding or impact, transition from the tetragonal (t) to monoclinic (m) phase can appear at normal temperatures, being followed by an increase of volume of at least 5%, causing compressive stress. If the stress exceeds a certain limit, deformation and mechanical failure will push the material to crack into

splinters. These limits are material specific, however, the mechanical properties and the stress intervals are specified in the BS EN ISO 13356/2013 [6], standard and every implant material should be designed in order to accomplish these specifications.
The main method used for the stabilization of the ZrO_2 tetragonal phase is the stabilization components in the zirconia lattice, such as Mg, Ce, Fe, Y, etc. At nanoscale level, the metastable phase formation in ZrO_2 can be induced by including in the oxide structure some vacancy defects [7]. Although, the stabilization effect of the oxygen vacancies in tetragonal ZrO_2 is not yet well understood (contrary to cubic ZrO_2) [8], the concentration of oxygen vacancies in the lattice required to stabilize the tetragonal phase is found in phases like $ZrO_{1.97}$ and $ZrO_{1.98}$ for tetragonal zirconia doped by rare-earth elements, mainly cerium (Ce) and yttrium (Y). The paper proposes to investigate the influence of the phase change of ZrO_2 ceramics following doping with Ce on the mechanical properties, knowing that Ce stabilized zirconia are characterized by excellent hydrothermal stability and high fracture toughness. By combining characterization techniques based on X-ray (XRD) and neutron diffraction (ND) and non-destructive evaluation methods based on Resonant Ultrasound Spectroscopy (RUS), we investigated the structure of these ceramics, for potential applications in the biomedical field.

2. Materials and methods

The Ce doped zirconia samples were sinterized using standard ceramic technology[6], starting from a mixture of ceria and zirconia oxides ($Zr_{1-x}Ce_xO_2$ (x = 0–0.17)) which are used in proportions established *a priori*. The samples have undergone a process of grinding and pressing in the form of cylinders and sinterized in air at a temperature of 1500 ^{0}C for a total of six hours. The phase composition as well as type of crystal structure of powder samples, were analyzed by conventional X-ray diffractometers (Xpert Pro MPD PANalytical diffractometer (Phillips) and a BRUCKER AXS D8- Advance diffractometer) with Cu-K_α radiation. A powder diffraction software package, which includes the standards of the Crystallography Open Database (COD)[9] was used to determine the phase composition. The structural analysis of ceramic samples $Zr_{1-x}Ce_xO_2$, was performed at room temperature using the time-of-flight High Resolution Fourier Diffractometer HRFD) instrument at the IBR-2 pulsed reactor in JINR Dubna, Russia[10]. At HRFD diffractometer, the correlation technique of data acquisition is used, which provides a very high resolution ($\Delta d/d \approx 0.001$). It is practically constant in a wide interval of d_{hkl} spacings [10]. The high-resolution diffraction patterns were collected by detector, placed at back scattering angles ($2\theta = \pm 152°$, d_{hkl} = 0.6 – 3.6 Å). For X-ray diffraction, a layer of typically 10 μm thickness has been investigated, whereas in the case of neutron diffraction, a thickness of tens of centimeters of a sample has been investigated. The crystalline structure constants, atomic positions were determined by FullProof Software. The crystallite shape and size has been characterized using SEM JSM-6490LV. RUS is a complex method that allows the determination of elastic constant [11-12] and the elements of elasticity matrix for samples with certain shapes [13-15]. Sample geometry affects data acquisition [16]. For cylinders with a high ratio of length to diameter, we have few excitation modes and the spectra are simple [17]. For the studied samples the ratio is around the unit and the spectrum requires more analysis than a long bar. The resonance frequencies of the samples have been analyzed using RUS technique. The frequency spectrum measured on the sample has visible resonance peaks for sample weakly dissipative media. The ceramic sample is supported by two identical piezoelectric

US sensors, placed at opposite edges of the ceramic cylinders (Figure 1).

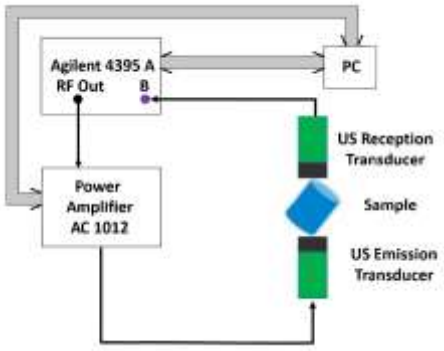

Figure 1. Experimental set-up for RUS-schematic block diagram

A Network/Spectrum/Analyzer 4395A Agilent USA generates a sweep frequency between 80 kHz and 240 kHz in 1 kHz step. The signal is amplified into a Power amplifier AC 1012 AG&TC Power Inc. USA and applied to the emission sensor P111.O.06P3.1 with large bandwidth. The signal delivered by the reception sensor is applied to the B port of the analyser, the spectrum being acquired by PC through numerical codes developed in Matlab 2014b. In order to determinate the elastic and shear moduli for samples, the propagation speed of longitudinal and transversal ultrasound waves were measured using transmission procedure and densities of the samples were obtained by means of Archimedes method, by using water as fluid [18].

3. Results and discussions

According to ND, the samples are not homogeneous and the structure is dependent on the Zr/Ce concentration [18]. The crystallite structures are presented in Figure 2, showing that the crystallites varies from 2-6 μm (in Figure 2b and c).

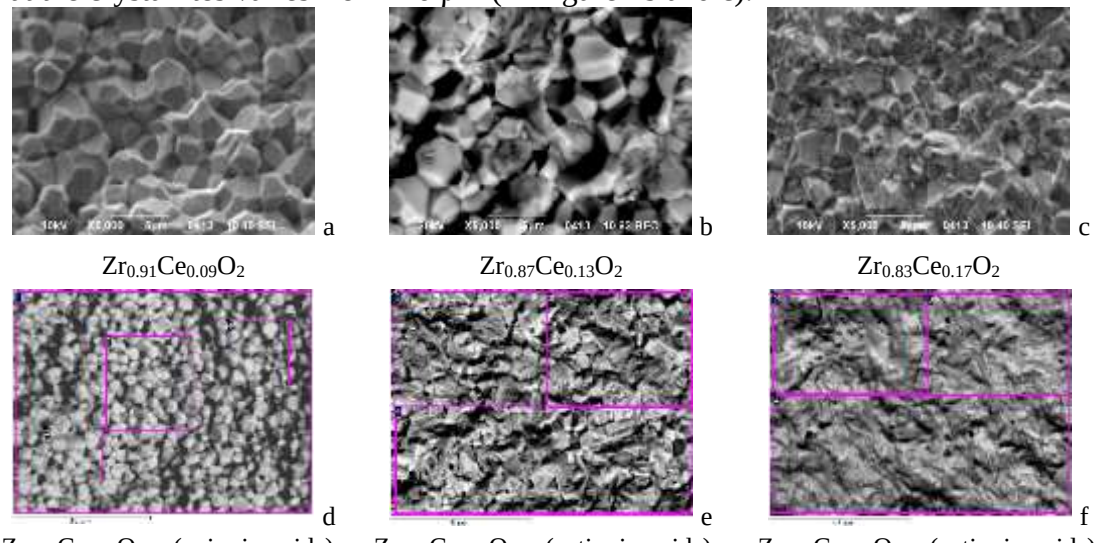

a $Zr_{0.91}Ce_{0.09}O_2$ b $Zr_{0.87}Ce_{0.13}O_2$ c $Zr_{0.83}Ce_{0.17}O_2$

d $Zr_{0.93}Ce_{0.13}O_{1.93}$ (anionic voids) e $Zr_{0.83}Ce_{0.13}O_{2.01}$ (cationic voids) f $Zr_{0.76}Ce_{0.19}O_{2.04}$ (cationic voids)

Figure 2. $Zr_{1-x}Ce_xO_2$ micrography: SEM (a-c); EDX determined (d-f)

The sample containing a Ce concentration of x=0.09 is formed by an agglomeration of crystallites which appears more faceted and pronounced, in contrast to the observed structure of the sample at compositions x=0.13 and x=0.17 where the shape of the

crystallites appears to be more planar and the faceting character is less evident. The electron microscopy indicated important change with the increase of Ce concentration [18]. Determination of chemical composition by EDX (the electrons bundle reach the sample, products a characteristic radiation for each element by the envisaged zone) (Figure 2 d; e and f) shows that the characteristic radiation intensity determines the concentration of each element from the envisaged zone. Several determinations were done for each sample and the average concentrations for each element were determined. X-ray diffractograms for the samples (nominal composition) are presented in Figure 3.

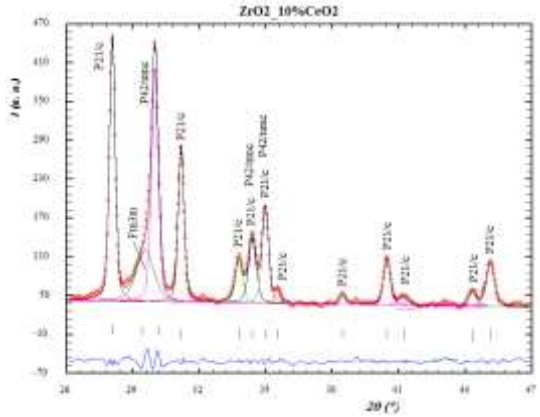

Figure 3. X-ray diffractogram of $Zr_{0.91}Ce_{0.09}O_2$ (nominal composition) Full Proof

The existence of three phases: cubic (space group Fm3m), tetragonal (space group $P4_{2/nmc}$) and monoclinic (space group $P2_{1/c}$) it is shown. In Table 1, a set of crystallographic features for each of the samples in the compositional range (x=0.09 – 0.17) is presented.

Table 1. Refined structural parameters of $Zr_{1-x}Ce_xO_2$ nominal composition at room temperature*

Parameters	x =0.09 (π2)			x =0.13 (π3)		x = 0.17 (π4)	
	Monoclinic P21/c	Tetragonal P42/nmc	Cubic Fm3m	Tetragonal P42/nmc	Cubic Fm3m	Tetragonal P42/nmc	Monoclinic P21/c
a, (Å)	5.3797	3.6276	5.220	3.6341	5.223	3.6362	5.1509
b, (Å)	5.2171	3.6276	5.220	3.6341	5.223	3.6362	5.2361
c, (Å)	5.1993	5.2190	5.220	5.2339	5.223	5.2458	5.2454
β, (^{0})	99.059	90.00	90.00	90.00	90.00	90.00	90.415
Vcell,	144.11	68.68	142.20	69.15	142.50	69.10	141.47
Volume fractio	0.514	0.412	0.164	0.826	0.174	0.552	0.448
D(Å)	198	180	-	514	140	368	120
$\varepsilon*10^3$	56	70	-	17	108	46	127
Rwp, %	14.3			10.4		10.4	

* obtained by processing the data collected using *BRUCKER AXS D8- Advance diffractometer with Cu-Kα radiation.* (x - the nominal Ce concentration; a,b, c – unit cell constants; β- angle of monoclinic unit cell; D – average size of crystalline blocks; ε- *microstrains* , V_{cell} – unit cell volume)

The relative concentrations of phases depend on the ratio between the Zr and Ce concentrations. Moreover, as the concentration of Ce is increasing, the unit cell volume of the monoclinic phase is decreasing, while the tetragonal unit cell slowly increases. Thus, the Ce concentrations influence on the characteristics of the resulting material, as

follows. The X-ray and ND of the compound $Zr_{1-x}Ce_xO_2$ (x=0.09-0.17) emphasize the fact that the samples are not homogeneous, and the phase composition and each phase of the investigated samples is dependent on the Ze/Ce ratio, example the XRD analysis for x=0.09. It is visible that the tetragonal phase is stabilized for all the compositions. The monoclinic phase exists in the far ends of the compositional range, and the cubic phase disappears at a composition of x=0.17. Neutron diffraction (ND) performed on $Zr_{1-x}Ce_xO_2$ (x=0.09-0.17) indicated that the sample corresponding to x=0.09 contains only two phases: one tetragonal ($P4_{2/nmc}$) and other monoclinic ($P2_{1/c}$) (Table 2). The increase of concentration of Ce ions leads to changing of crystal structure from monoclinic to tetragonal ($P\ 4_{2/nmc}$) with two formula units (Z=2) per unit cell -Table 2.

Table 2. Refined structural parameters of $Zr_{1-x}Ce_xO_2$ at room temperature**

x	x =0.09		x = 0.13	x = 0.17
Parameters	Monoclinic $P2_1/c$	Tetragonal $P4_2/nmc$	Tetragonal $P4_2/nmc$	Tetragonal $P4_2/nmc$
a, (Å)	5.2039	3.6233	3.6358	3.6452
b, (Å)	5.2148	3.6233	3.6358	3.6452
c, (Å)	5.3767	5.2159	5.2378	5.2471
β, (^{0})	98.938	90.0	90.0	90.0
Vcell, (Å3)	144.140	68.476	68.238	69.720
R, %	14.0		10.4	10.4

** obtained by processing the data collected using the High Resolution Fourier Diffractometer (neutron diffractometer) at IBR-2 reactor FLNP-JINR.

We consider that the difference between the XRD results and ND results are due to a change of the chemical composition of the samples, which have other chemical composition at surface comparing with the bulk samples. Interaction of ultrasounds with microscopic inhomogeneities of materials causes noise dispersion and attenuation, (i.e. the scattered wave amplitude modification) and can be used to evaluation of the materials. Due to the scattered on the microstructure of materials, the detection and evaluation of defects is difficult, the so-called structural or granular noise overlaps the defect signals, and the dispersion of velocity prevents exact positioning of the defects. This suggests the need to apply complementary methods of non-destructive evaluation.

RUS is based on the principle that the mechanical resonant response of solids depend strongly on its elastic moduli, shape and density. Resonant (or natural) frequencies of a system can be either measured or calculated by solving equations of motion for the known shape [19-20]. The reverse is also true; if resonant frequencies of an object are known, its elastic properties can be determined [21]. Quality of the object may be identified from a resonant frequency spectrum by resonant frequency shifts, peak splitting, increases in peak width and changes in amplitude. The method is based on the estimation of resonant eigenfrequencies [17], based on an eigenvalue and eigenfunction method [22]. It is evident that the solutions of the eigenvalue and eigenfunction problem can only be found via numerical methods. The resonance spectra for the studied samples were traced for a frequency range 80kHz to 240kHz (Figure 4). Due to the fact that the samples π_2 - π_4 are axisymmetric, isotropic and homogeneous [22], every mode observed on samples must fall into the following three categories [23]:

- Torsional axisymmetric pure share motion consisting of rigid rotation of rings of materials around the sample axis. The frequency of these modes depend strongly on the sample's shear velocity

- Extensional axisymmetric mixtures of compression and shear modulus
- Flexural modes along paths that are tilted with respect to the cylinder axis. These modes occur in pairs named doublets, with the same resonance frequency.

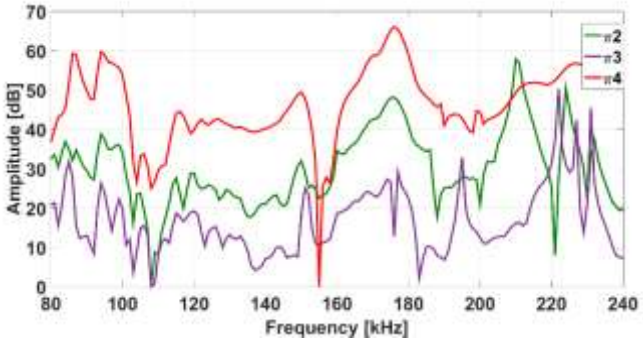

Figure 4. Resonance ultrasound spectra for samples (π_2, π_3, π_4)

The RUS spectrum describes a large amplitude response detected when the frequency corresponds to one of the samples eigenfrequencies. The amplitude responses in the swept frequency range are in tight connection to the sample's properties, especially the ones related to the density. The eigenfrequency intervals exhibit a slight shift towards smaller values as the density of the samples decrease according to value presented in Table 2.

Figure 5 present resonant modes for sample π_2 in a frequency range 80 kHz to 240 kHz for two extensional modes (a and b) and two flexural modes, (c and d). The simulations using SolidWorks 2015, Simulation-Frequency toolbox using a solid mesh type, curvature based meshing use 13145 nodes and 8777 total elements. The resonance frequency obtained by simulations agreed with experimentally ones chosen at full width at half maximum of the amplitude [22].

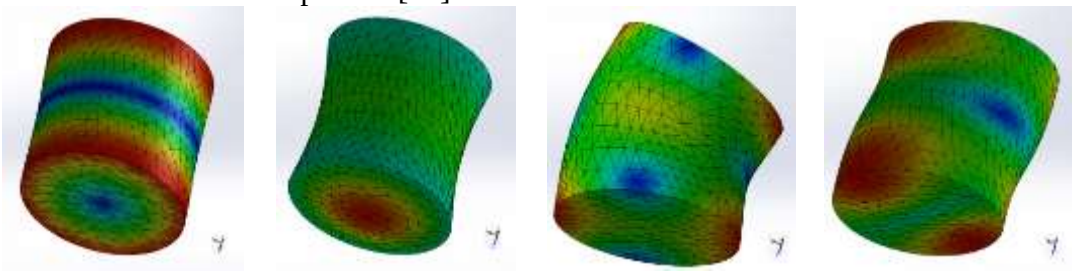

a b c d

Figure 5. Resonant modes for sample π2: (a) extensional mode, f= 163 kHz; (b) extensional mode, f=185 kHz; (c) flexural mode f=208 kHz; (d) flexural mode f=214 kHz.

The simulated information are used to determine which of the resonances are observables in the experimentally obtained spectrum. According to [17] the inversion of data has been used in order to determine the elastic properties from the measured resonance spectra, using the conjugate gradient method with minimizing the objective function.

The maximum displacements appear as red patches in the above representations, the intermediate ones appear in yellow and green and the minimum ones appear in blue. It is noticeable that for the analysed frequencies, the maximum displacements take place at the edges of the cylinders in opposite directions, with a minimum in the middle of the samples. The inversion was only applied to determine the elastic modulus (E) and shear modulus (G) and not the geometrical dimensions and densities of the samples. An increase of the relative density with Ce concentration take places (Table 3).

Table 3. Some crystallographic and mechanical characteristics of $Zr_{1-x}Ce_xO_2$ samples

Ce concentration (x)	Molecular Mass	Crystallographic Structure (ND)	Relative Density (%)	Elasticity Modulus (GPa)	Shear Modulus (GPa)	Poisson Ratio
0.09	127.62	monoclinic + tetragonal	88.9	145.85	56.49	0.291
0.13	129.58	tetragonal	94.7	168.53	64.47	0.307
0.17	131.53	tetragonal	99.9	193.43	73.16	0.322

We considered that a decrease of the pores concentration takes place with the increase of the Ce concentration in the samples.

4. Conclusions

The zirconia ceria mixed oxide, solution combines the mechanical and thermal stability zirconia with the variable oxidation state of ceria, leading to an enhanced structural stability. The phase of $Zr_{1-x}Ce_xO_2$ (x=0 – 0.17) can be changed by replacing Zr with Ce. A progressive transition between the monoclinic and the tetragonal phases was observed, as well as a compositional difference between the surface layer and the bulk sections of studied samples. This difference can be attributed to various oxygen concentrations between the surface layer and the bulk sample. A set of complementary methods for the determination of crystallographic and mechanical characteristics of this class of ceramics were employed. Using RUS for quality control, whose ratio is around the unit, the interpretation is favorable because the torsional mode is the lowest one, well separated from the others for Poison's ratio bigger than zero, allowing extraction of the shear modulus and its damping. If the elements are incorrectly sintered, with a density smaller than the prescribed value and the elastic and shear moduli smaller, important modifications appear in the spectrum and the resonance frequencies. Slight material anisotropy leads to splitting of the higher modes but not of the fundamental torsion mode. An increase of the relative density and of the mechanical parameters was obtained with the increase of Ce concentration, promoting these compounds for medical prosthesis applications.

Acknowledgements

This paper is partially supported by Ministry of Research and Innovation under UEFICDI Grant PN-III-P1-1.2-PCCDI-2017-0239, Nucleus Program PN 18060102.

References

1. SC Cowin, "Bone Mechanics Handbook", 2nded., CRC Press, Boca Raton, USA 2001
2. RE Kennon, JM Keggi, RS Wetmore, LE Zatorski, MH Huo, KJ Keggi, "Total hip arthroplasty through a minimally invasive anterior surgical approach", J Bone Joint Surg 85-A(4), pp.39-48, 2003.
3. KO Onuoha, M Solow, JM Newman, N Sodhi, R Pivec, A Khlopas, AA Sultan, M Chughtai, NV Shah, J George, MA Mont, "Have the annual trends of total hip arthroplasty in rheumatoid arthritis patients decreased?" Ann Transl Med 5(3), 2017.
4. D Granchi, LM Savarino, G Ciapetti, N Baldini, "Biological effects of metal degradation in hip arthroplasties", Crit Rev Toxicol. 48, 2, pp. 170-193, 2018.
5. SE Kulkova, ON Muryzhnikova, "Electronic structure and optical properties of

zirconia", Inorg Mater 36(1), pp.38-42, 2000.
6. ISO 13356–2015 Implants for surgery - Ceramic materials based on yttria-stabilized tetragonal zirconia (Y-TZP).
7. WZ Zhu, "Effect of cubic phase on the kinetics of the isothermal tetragonal to monoclinic transformation in ZrO_2 (3 mol% Y_2O_3) ceramics", Ceram Int 24, pp.35-43, 1998.
8. PLi, I Chen, JE Penner-Hahn, "Effect of Dopants on Zirconia Stabilization-An X-ray Absorption Study: I, Trivalent Dopants", J Am Ceram Soc 77, pp.1289–1295, 1994.
9. Crystallography Open Database. Available online: http://www.crystallography.net
10. AM Balagurov, "Scientific Reviews: High-Resolution Fourier Diffraction at the IBR-2Reactor", Neutron News 16, pp. 8–12, 2005.
11. A Migliori, J L. Sarrao, "Resonant ultrasound spectroscopy: applications to physics, materials measurements, and nondestructive evaluation", Wiley, 1997
12. MC Remillieux, TJ Ulrich, C Payan, J Rivière, CR Lake, PY Le Bas, "Resonant ultrasound spectroscopy for materials with high damping and samples of arbitrary geometry" J Geophys Res-Sol Ea 120(7), pp.4898-4916, 2015.
13. TJ Ulrich, KR McCall, RA Guyer, "Determination of elastic moduli of rock samples using resonant ultrasound spectroscopy", J Acoust Soc Am 111(4), pp.1667-74, 2002.
14. VM Visscher, A Migliori, TM Bell, RA Reinert, "On the normal modes of free vibration of inhomogeneous and anisotropic elastic objects", J Acoust Soc Am 90, pp.2154-62,1991.
15. A Migliori, JD Maynard, "Implementation of a modern resonant ultrasound spectroscopy system for the measurement of the elastic moduli of small solid specimens", Rev Sci Instrum 76, 121301, 2005.
16. TR Jaglinski, S Lakes, "Resonant ultrasound spectroscopy of cylinders over the full range of Poisson's ratio", Rev Sci Instrum 82(3) 035105, 2011.
17. DV Myasnikov, AV Konyashkin, OA Ryabushkin, "Identification of eigenmodes of volume piezoelectric resonators in resonant ultrasound spectroscopy", Tech Phys Lett 36, pp. 632–635, 2010.
18. A Savin, ML Craus, V Turchenko, A Bruma, PA Dubos, S Malo, TE Konstantinova, VV Burkhovetsky, "Monitoring Techniques of Cerium Stabilized Zirconia for Medical Prosthesis", Appl Sci 8, 5(4), pp.1665-82, 2015.
19. BR Goodlet, CJ Torbet, EJ Biedermann, LM Jauriqui, JC Aldrin, TM Pollock, "Forward models for extending the mechanical damage evaluation capability of resonant ultrasound spectroscopy", Ultrasonics, 77, pp. 183-196, 2017.
20. CW De Silva, "Vibration: fundamentals and practice" CRC Press: Boca Raton, 2000.
21. F Ren, ED Case, A Morrison, M Tafesse, MJ Baumann, "Resonant ultrasound spectroscopy measurement of Young's modulus, shear modulus and Poisson's ratio as function of porosity for alumina and hydroxyapatite" Philos Mag 89(14), pp.1163-82, 2009.
22. BJ Zadler, JH Le Rousseau, JA Scales, ML Smith, "Resonant ultrasound spectroscopy: theory and application", Geophys J Int 156(1), pp.154-169, 2004.
23. HH Demarest Jr, "Cube-Resonance Method to Determine the Elastic Constants of Solids" J Acoust Soc Am 49(3B), pp. 768-775, 1971.